FAILURE ANALYSIS OF METAL OXIDE ARRESTERS UNDER HARMONIC DISTORTION

P. Bokoro* **and I. Jandrell†**

* *University of Johannesburg, Dept. of Electrical Engineering Technology, 37 Nind Street, University of Johannesburg, South Africa E-mail: pitshoub@uj.ac.za*

† *Faculty of Engineering and the Built Environment, Private Bag 3, Wits 2050, South Africa E-mail: ian.jandrell@wits.ac.za*

Abstract: The probability of accelerated degradation or reduced time to failure of metal oxide arresters (MOA), when continuously exposed to distorted ac conduction, is analysed in this study. Metal oxide-based surge arresters of similar size and electrical characteristics are tested using accelerated degradation at elevated temperature and distorted ac voltage stress. The three-parameter Weibull probability method is applied to analyse the obtained time to failure distribution. The Fourier series' expansion is also relied upon in order to evaluate the content of the harmonic resistive components of the measured leakage current. The results obtained indicate that for 6.24% and 5.58% content of the 3^{rd} and the 5^{th} harmonic component, respectively embedded in the applied voltage stress, the probability of reduced time to failure or accelerated degradation is found to be 58.93 %, and the mean life reduction obtained is just above 40%. These results correlate with the pronounced shift of the $U-I$ curve as well as the increase in the magnitude of the respective harmonic resistive current components of the arrester samples.

Key words: Time to failure, metal oxide arrester, voltage harmonics, resistive current, reliability.

1. INTRODUCTION

Metal Oxide arresters (MOA) experience electrical degradation or ageing as a result of continuous ac or dc conduction [1-3]. The degradation phenomenon refers to irreversible change in electrical and physical properties of the MOA components [4, 5], and consists of one of the most encountered failure modes that affect metal oxide-based arrester components [6, 7]. With the prevalence of harmonic-producing loads in modern electrical networks, MOA devices are likely to be continuously exposed to voltage and current harmonic frequencies. Previous studies described in [8-11], have indicated the impact of voltage harmonics on the leakage current-based condition assessment of metal oxide-based surge arresters. The major shortcoming in these studies is the probable aggravated degradation or failure process of these surge protection devices as a result of voltage and current harmonics in the power system. In the present work, two commercially-sourced sets of MOA are tested and analysed. Each set consisted of 60 units of similar physical and electrical characteristics. These arrester components are subjected to accelerated degradation test at 135^oC for a time period of 96 hours. The applied voltage stress consisted of distorted waveform whose fundamental component amounted to 85 % of the ac rated breakdown voltage ($0.85U_{1mAac}$) of the MOA. The 3^{rd} and 5^{th} harmonic voltage components are found to be prominent in the applied voltage stress, and their percentage content is considerably changed when the harmonic source used in this study is removed from the circuit. The results obtained show that arrester samples subjected to voltage stress, containing higher harmonic content, exhibit higher probability of failure or degradation, and significant rise in the magnitude of the resistive harmonic current components.

2. EXPERIMENTAL WORK

For the metal oxide-based arresters used in this study, two separate types of test set up are applied: the accelerated degradation test at elevated voltage and temperature, which emulates real life arrester deterioration process [12], and the dc voltage-current $(U-I)$ test for the purpose of reference voltage (U_n) measurement, which enables the degradation or failure status of arresters to be verified.

2.1 The accelerated degradation test

This test regime essentially consisted of the following components: a heat chamber or mini-furnace, a 50 Hz ac supply voltage, the triac - based voltage controller (harmonic source), a resistive load, high-temperature conductors, data logger units and FN 2090 single-phase multi-purpose filter. The heat chamber consisted of the Nabertherm P330 with 9 settable heating programs or courses (P1-P9), and 40 time-segments grouped in blocks of 10 (A-J)[13]. Each block is made up of 4 time-segments (2 ramp and 2 holding times). A heating program could be formed of one or more blocks. In this study, the desired temperature is reached at the first holding time-segment (t_{2B}) of block B, which is assigned a time value of 96 hours and a temperature of 135^oC. The subsequent time-segments are therefore assigned a zero value. At the end of the degradation time thus set, the unit will automatically switch off and enter the waiting time or cooling mode. The heating program used in this study is shown in figure 1.

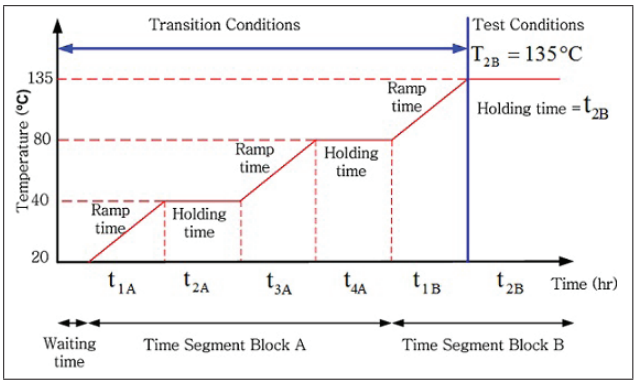

Figure 1: Heating Program

When the triac-based voltage controller is removed from the circuit, and the multi-purpose filter is connected: the non-linear leakage current resulting from high conduction through MOA devices induced 1.89 % of the 3^{rd} and 2.5% of the 5^{th}, which fall within the permissible level of harmonic [14]. Upon the connection of the triac-based voltage controller, these harmonic components increased to values beyond permissible level: 6.24 % and 5.58 %, respectively. The set up of the accelerated degradation test is provided in figure 2.

Figure 2: Accelerated Degradation Test Set up

Each test run accommodates five MOA samples connected across terminals, mounted in parallel on a concrete platform inside the heat chamber. These terminals are supplied through 1.5 mm^2 high-temperature single-core silicon cables (Silflex), capable to withstand 180^{o}C [15]. The supply voltage is controlled from an external timer unit set to trigger when the chamber reaches 135^{o}C of temperature. To prevent any event of short circuit, protective fuses rated 250 V; 0.125 A are connected in series with each test sample. A three channel K5020 and 2 x MT250 data logger units are connected in such a way that voltage events across each sample are recorded. The TDS 1001B two-channel Tektronix and the 4-channel Rigol digital scopes are used to monitor the supply voltage and to record the leakage currents, with the aid of 5/1 A current transformers and a current probe. The failure or breakdown times measured in both test conditions are extrapolated, using the Arrhenius model, to time values (t_i) corresponding to long-term operation of these devices at service condition: 40^{o}C at maximum condition operating voltage (MCOV). Prior to the estimation of the shape and scale parameters of the obtained time to failure distributions, such as described in the IEEE guide for statistical analysis of insulation breakdown [16]. The applied voltage and leakage currents are measured during the test, in comma separated values (CSV) format using the Rigol DS1204B digital scope. The Fourier series expansion technique is applied to determine the magnitude of the harmonic resistive current components in measured leakage current waveforms. The $U-I$ characteristic curves of the tested samples are also plotted. The voltage stress applied to arresters (without external harmonics) was provided through FN 2090 single-phase and multi-purpose filter, in a bid to reduce harmonics from the mains. A 83.3 $k\Omega$ resistive load was connected across the filter and outside the heat chamber. The time-domain of the continuous voltage stress applied under this condition is indicated in figure 3.

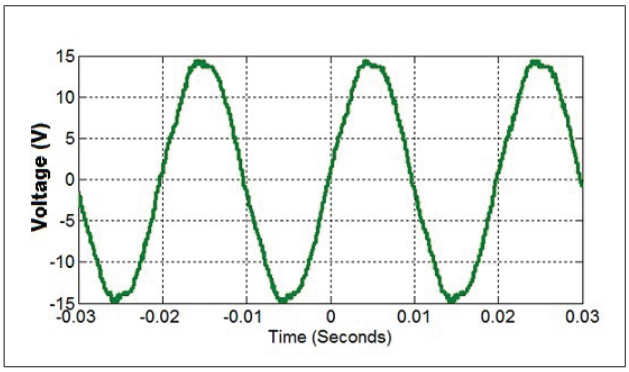

Figure 3: Applied Voltage Stress (no external harmonic source)

The harmonic components in the voltage stress resulting from non-linear current conduction through arrester components are shown in figure 4. To introduce harmonic distortion from an external harmonic source, the triac-based voltage controller is brought in to effect the switching of the resistive load, the applied voltage stress therefore experiences much higher harmonic distortion. This is shown in figure 5. The resulting voltage harmonic components in the applied stress, when an external source of harmonic is depicted in figure 6.

2.2 *Description of Arrester Samples*

The overvoltage protection samples used in this work consisted of low-voltage MOA units with 20 mm of diameter size. The mean resistance (R_{mean}), inductance (L_{mean}) and capacitance (C_{mean}) of the varistor arresters are measured at room temperature, using an ELC-131D LCR meter. The breakdown voltage (U_{1mAac}) as well as the MCOV (U_{ac}) of the MOA devices are obtained from the manufacturer [17]. The electrical properties or characteristics of the tested arresters, such as specified in

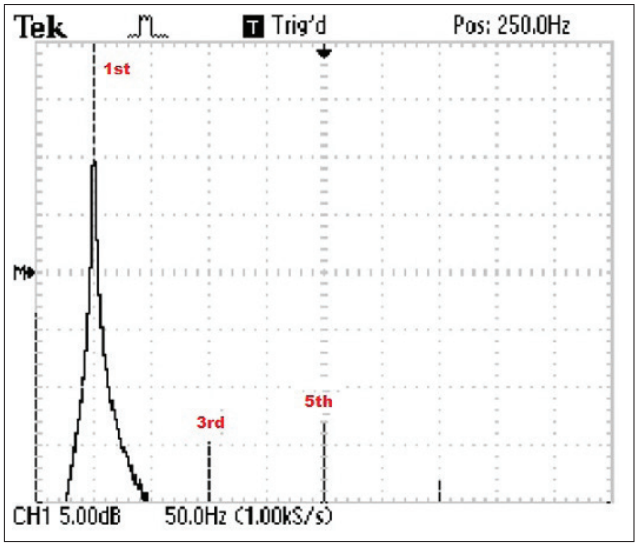

Figure 4: Frequency Components of the applied voltage stress (No external harmonic source)

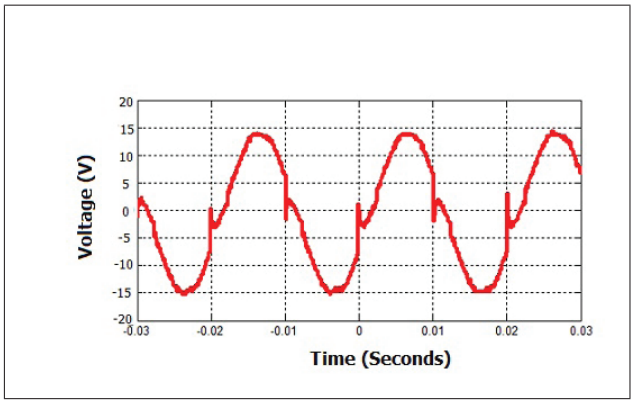

Figure 5: Applied Voltage Stress (with external harmonic source)

the manufacturer's data book, are provided in table 1.

2.3 $U-I$ Measurement of MOA Samples

The $U-I$ characteristic curve of MOA samples is measured at room temperature using a variable dc source. The arrester is therefore connected across the output. A volt and current meter are respectively connected across and in series with the device under test. The measurement points obtained are subsequently used to plot the $U-I$ characteristic curve. This test is conducted before and after accelerated degradation test at room temperature. The reference voltage (U_n) and the standby leakage current (I_{L_o}), which is defined as the current measured at 85% of the reference voltage [18, 19], could therefore be obtained. The mean $U-I$ curve of the samples before and after degradation test are provided in figure 7.

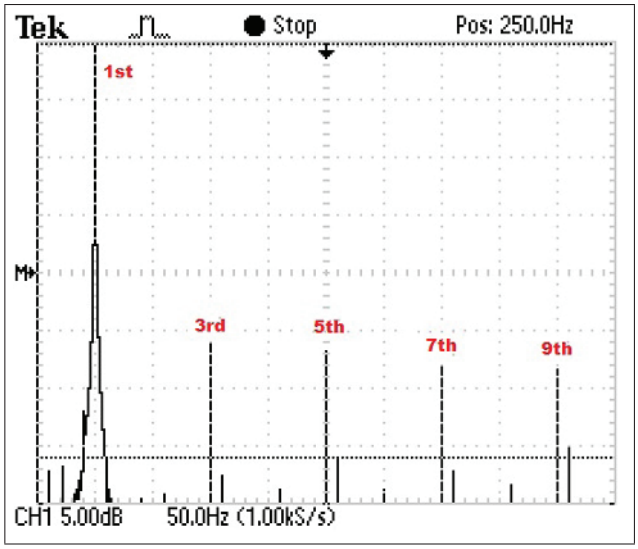

Figure 6: Frequency Components of the applied voltage stress (With external harmonic source)

Table 1: Electrical Characteristics of Arrester Samples

Characteristics	Values	Units
R_{mean}	5.6	MΩ
L_{mean}	18.04	H
C_{mean}	1225	pF
U_{1mAac}	205	V
U_{ac}	130	V

3. WEIBULL PLOTS

3.1 Time data obtained:

The procedure followed to obtain the time to failure distribution and the resulting probability functions is summarised in figure 8. The failure times (t_i) measured during accelerated degradation tests and the change in the dc reference voltage ($\triangle U_n$), are used to isolate the survived and spoiled components from the failed arrester samples, on the basis of the following conditions:

1. Failed samples: $t_i \leq t_{2B}$ and $\triangle U_n \geq 5\%$
2. Survived samples: $t_i = t_{2B}$ and $\triangle U_n < 5\%$
3. Spoiled samples: $t_i < t_{2B}$ and $\triangle U_n < 5\%$

The classification of arrester samples as result of the above conditions is shown in table 2. Using the Arrhenius accelerating factor [20], the time-points measured for the failed samples are extrapolated to unit values corresponding to equivalent operation of arresters at standard temperature of 40^{o}C.

$$[t_{eq.40^oC}]_i\,[hours] = t_i \times 2.5^{\frac{T_{2B}-40}{10}} \quad (1)$$

Where:

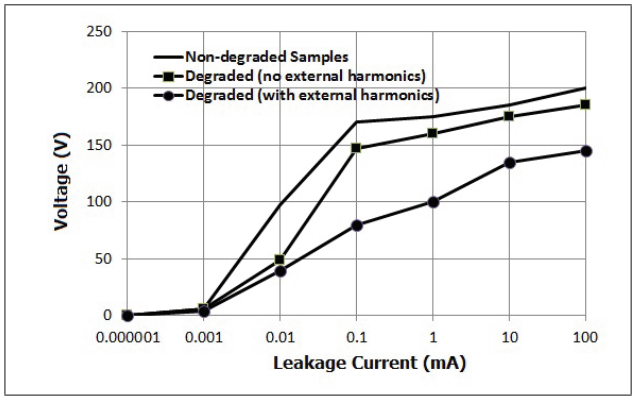

Figure 7: Mean U-I curve of Arrester Samples

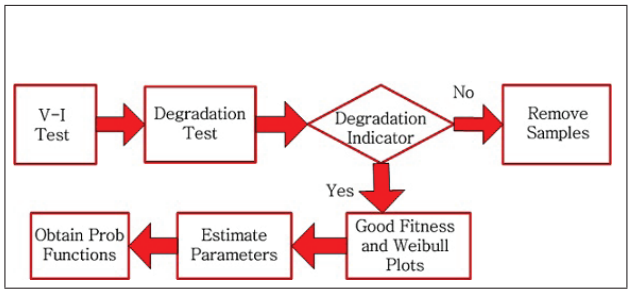

Figure 8: Block Diagram of Failure Probability Analysis

$[t_{eq.40^oC}]_i$ = time equivalent to arrester operation at 40^{o}C or service condition
T_{2B} = the test temperature.

Each failure time is assigned a ranking number (i) which counts the number of failures in a given time, and ultimately the number of failed arresters at any indicated time. This helps to determine the percentage cumulative failure probability using White's approximation [21, 22].

$$F(i,n) \approx \left(\frac{i-0.44}{n+0.25}\right) \times 100 \qquad (2)$$

Where:

$F(i;n)$ = the percentage cumulative failure probability
i = the number of failures in a given time
n = the number of tested samples.

The Weibull cumulative distribution function (CDF) of both sample groups, can therefore be plotted on the basis of $[t_{eq.40^oC}]_i$ and $F(i,n)$. The CDF of arresters exposed to no external harmonic source and that of those subjected to an external harmonic source are shown in figures 9 and 10, respectively.

Table 2: Classification of degraded Samples

Samples	No harmonic source	With harmonic source
Failed	27	37
Survived	30	18
Spoiled	3	5

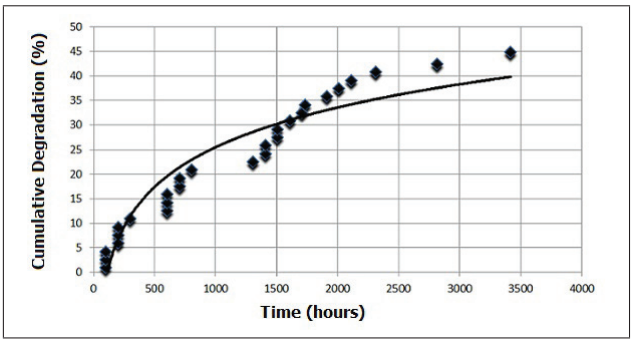

Figure 9: CDF (Sample without external harmonics)

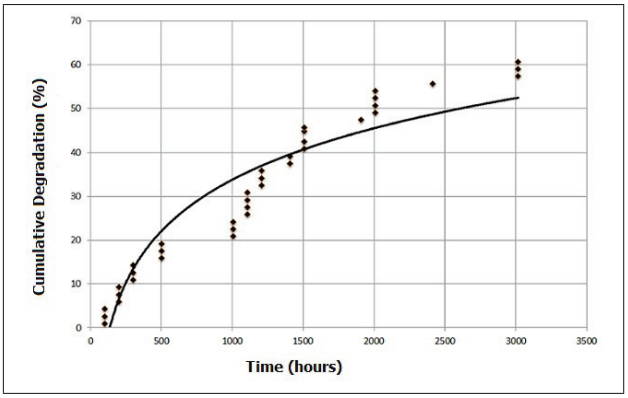

Figure 10: CDF (Sample with external harmonics)

3.2 *Adequacy of the Distribution:*

To test the adequacy or the goodness of fit of the distributions obtained, both the $F(i;n)$ and $[t_{eq.40^oC}]_i$ are assigned respective logarithmic expressions x_i and y_i as indicated in [23, 24]. These values are determined from the following equations:

$$x_i = \ln\left[-\ln\left(1-\frac{F(i,n)}{100}\right)\right] \qquad (3)$$

Where:

x_i = the logarithmic expression of the percentage cumulative failure probability

And:

$$y_i = \ln\left(t_{eq.40^oC}\right)_i \qquad (4)$$

Where:

y_i = the logarithmic expression of the time equivalent to arrester operation at 40^{o}C or service condition.

The x_i and y_i values are used to determine the correlation factor, which should be equal or higher than the Weibull critical coefficient value (γ) for a curve to be deemed fit or adequate [23]. The correlation factor is calculated using the correlation function equation [25], expressed as follows:

$$\gamma(x_i, y_i) = \frac{\sum (x_i - \bar{x}) \cdot (y_i - \bar{y})}{\sqrt{\sum (x_i - \bar{x})^2 \cdot \sum (y_i - \bar{y})^2}} \tag{5}$$

Where:

$\gamma(x_i, y_i)$ = the correlation function
$\bar{x}$ = the mean logarithmic value of the percentage cumulative failure probability ($\frac{\sum x_i}{r}$)
$\bar{y}$ = the mean value of the time equivalent to arrester operation at 40^{o}C or service condition ($\frac{\sum y_i}{r}$)
r = the number of failed arresters.

The correlation factors of the distributions obtained, using equation 5 are: $\gamma_1 = 0.955857$ and $\gamma_2 = 0.958317$. Based on the Weibull critical coefficient values provided in [23], both curves show good adequacy or fit to the Weibull distribution.

3.3 Estimation of the Weibull Parameters:

The least-squares regression method is used to determine the slope $m(x_i, y_i)$ and the c-intercept functions of the plotted curves [23, 24]. These functions are in turn used to estimate the shape and the scale parameters. The slope function is determined in equation (6), as follows:

$$m(x_i, y_i) = \frac{\sum (x_i - \bar{x}) \cdot (y_i - \bar{y})}{\sum (x_i - \bar{x})^2} \tag{6}$$

Where:

$m(x_i, y_i)$ = the slope function of the Weibull distribution.

Therefore, the shape parameter β is expressed as:

$$\beta = \frac{1}{m(x_i, y_i)} = \frac{\sum (x_i - \bar{x})^2}{\sum (x_i - \bar{x}) \cdot (y_i - \bar{y})} \tag{7}$$

Where:

β = the shape parameter of the Weibull distribution.

The c-intercept function is calculated using equation 8, given below:

$$c = \bar{y} - m(x_i, y_i) \cdot \bar{x} \tag{8}$$

Where:

c = the c-intercept function.

The scale parameter is therefore obtained using the exponential of the c-intercept function. This yields the following expression:

$$\alpha = \exp c = \exp [\bar{y} - m(x_i, y_i) \cdot \bar{x}] \tag{9}$$

Where:

α = the scale parameter of the Weibull distribution.

Applying equations 6,7,8 and 9 yield the scale and shape parameters of the time to failure distribution with and without harmonics to be determined: $\beta_1 = 0.98$ and $\alpha_1 = 4167.6$ hours, and $\beta_2 = 1.093$ and $\alpha_2 = 2746.5$ hours. For both distributions, the minimum time to failure or the location parameter $\gamma = 100.6$ hours, has the same value.

4. FAILURE ANALYSIS

Based on the three-parameter Weibull distributions obtained respectively for each set of degraded arresters (with and without harmonics), the probability density function (PDF) can be determined and subsequently analysed. Equation 10 is therefore applied:

$$f(t, \beta, \alpha, \gamma) = \frac{\beta}{\alpha} \cdot \left(\frac{t-\gamma}{\alpha}\right)^{\beta-1} \exp\left(-\frac{t-\gamma}{\alpha}\right)^{\beta} \tag{10}$$

Where:

$f(t, \beta, \alpha, \gamma)$ = the probability density fucnction
$\frac{\beta}{\alpha} \cdot \left(\frac{t-\gamma}{\alpha}\right)^{\beta-1}$ = the hasard or failure rate function
$\exp\left(-\frac{t-\gamma}{\alpha}\right)^{\beta}$ = the reliability function.

The PDF, the failure rate and the reliability functions of MOA samples degraded with and without harmonics are noted as follows: $f_1(t)$, $h_1(t)$, $R_1(t)$, $f_2(t)$, $h_2(t)$ and $R_2(t)$, respectively. To determine whether or not electrical failure of arrester units is indeed accelerated, as a result of external harmonic content in the applied voltage stress, the reliability, the failure rate and the PDF of these components under the testing conditions could be analysed. Therefore, the following statements apply:

1. The probability of one population of tested arresters to experience longer time to failure over the other is verified on the basis of the following probability condition [25]:

$$Pr[t_2 \geq t_1] = \int_0^{\infty} f_1(t) \cdot R_2(t)\, dt > 0.50. \tag{11}$$

Where:

$Pr[t_2 \geq t_1]$ = the probability that the population of arresters degraded with harmonics may experience longer time to failure.

2. The mean time to failure (MTTF) of the two populations of degraded arresters could also be analysed in a bid to determine the probability of higher survival rate or reliability of one population over the other [26].

$$\int_0^\infty \exp\left(-\frac{t-\gamma}{\alpha_2}\right)^{\beta_2} dt > \int_0^\infty \exp\left(-\frac{t-\gamma}{\alpha_1}\right)^{\beta_1} dt \quad (12)$$

3. The plots of the failure rate functions as applied to the degraded arrester populations must therefore be such that: $h_2(t) < h_1(t)$. This could be graphically demonstrated.

The above statements are therefore analysed to assess any probability of accelerated failure as a result of harmonics in the applied voltage stress.

5. LEAKAGE CURRENT ANALYSIS

Long-term exposure of varistor arresters to continuous voltage stress generally lead to failure of these devices. This is usually diagnosed in terms of increased magnitude of harmonic resistive component, and most particularly the third harmonic resistive current (THRC) component of the leakage current [27-30]. In order to assess the contributions of each voltage harmonic frequency, the leakage current of the degraded arrester populations is measured and captured in CSV format of the Rigol DS1204B digital scope. The time-domain waveform of the leakage current for arresters degraded without harmonics is shown in figure 11.

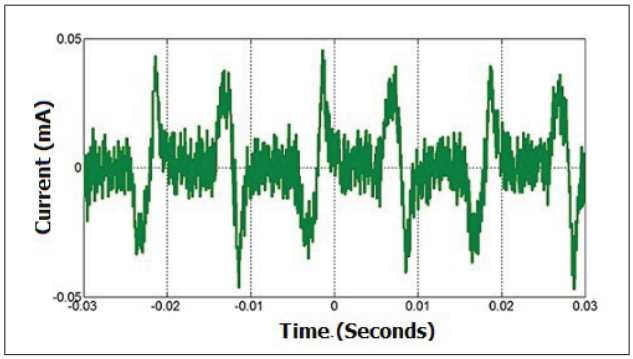

Figure 11: Leakage current waveform (Arresters degraded without harmonics)

Similarly, the time-domain waveform of the leakage current for arresters degraded with harmonics is indicated in figure 12.

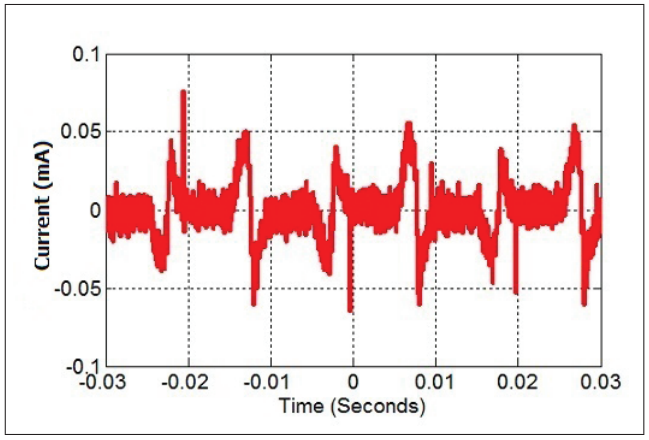

Figure 12: Leakage current (Arresters degraded with harmonics)

The current waveforms measured could be expressed in terms of frequency components using Fourier series' expansion, given the periodical behaviour of these current functions. This implies that:

$$i(t) = \frac{a_o}{2} + \sum_{k=1}^{\infty} (a_k \cos \omega_k t + b_k \sin \omega_k t) \quad (13)$$

Where:

$i(t)$ = the leakage current function

$a_o = \frac{2}{T}\int_0^T i(t)\,dt$

$a_k = \frac{2}{T}\int_0^T i(t)\cdot(coskt)\,dt$

$b_k = \frac{2}{T}\int_0^T i(t)\cdot(sinkt)\,dt$

T = the period of the function.

In order to evaluate the terms of equation (13), the time-domain curve of the leakage current is divided up into 20 equal time-intervals between 0 and T. The current values corresponding to the time points are sourced from the CSV measurement of the leakage current. The Fourier expansion of the leakage current function defined in equation 13 could be rewritten as follows:

$$i(t) = \frac{I_o}{2} + \sum_{k=1}^{\infty} \sqrt{2} I_k sin(\omega_k t + \phi_k) \quad (14)$$

Where:

$I_k = \sqrt{a_k^2 + b_k^2}$ = the RMS value of $i(t)$

$\omega_k = \frac{2k\Pi}{T}$ = the angular frequency

$\phi_k = \arctan\frac{a_k}{b_k}$ = the respective phase angle for the k^{th} current harmonic frequency component.

The Fourier expansion such as defined above is also extended to the applied voltages measured across MOA

samples during degradation test. This yields the following voltage expression:

$$v(t) = \frac{V_o}{2} + \sum_{k=1}^{\infty} \sqrt{2} V_k sin(\omega_k t + \theta_k) \quad (15)$$

Where:

$V_k = \sqrt{a_k^2 + b_k^2}$ = the RMS value of $v(t)$
$\omega_k = \frac{2k\Pi}{T}$ = the angular frequency
$\theta_k = \arctan \frac{a_k}{b_k}$ = the respective phase angle for the k^{th} voltage harmonic frequency component.

Since the power losses resulting from distorted voltage across MOA units could be estimated by the sum power losses of each components [31]. The instantaneous power $p(t)$ could therefore be expressed as the product of equations (14) and (15). Disregarding the dc components in both (14) and (15), the following equation is obtained:

$$p(t) = \sum_{k=1}^{\infty} \sqrt{2} I_k sin(\omega_k t + \phi_k) \cdot \sqrt{2} V_k sin(\omega_k t + \theta_k) \quad (16)$$

Where:

$p(t)$ = the instantanous power.

Developing further equation (16) yields the active or resistive component (P_R) of the total power absorbed by the arrester:

$$P_R = \sum_{k=1}^{\infty} V_k I_k cos(\theta_k - \phi_k) \quad (17)$$

Where:

P_R = the average power.

The magnitude of the fundamental and harmonic resistive components constituting the leakage currents could be effectively determined using the expression $I_k cos(\theta_k - \phi_k)$. The fundamental, the third and fifth harmonic resistive current components are shown in figure 13.

6. RESULTS AND DISCUSSION

Based on the mean $U - I$ characteristic curve obtained, arrester population degraded with harmonics proved to have the lowest decrease $(100V)$ in the reference voltage $(\triangle U_n)$ measured at 1 mA dc and at room temperature. Whereas arresters degraded without external source of harmonics have experienced a decrease of about 150 V in the reference voltage. This implies that the electrical stability of arresters degraded with harmonics is severely compromised as shown in figure 7. Based on the

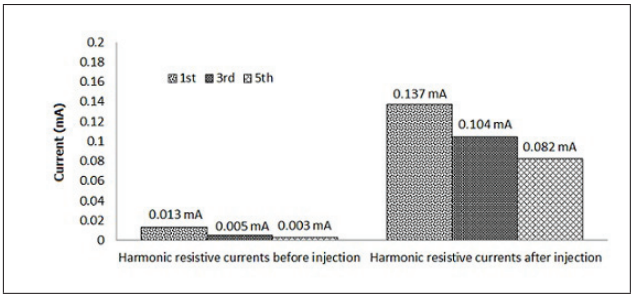

Figure 13: Resistive Current Components before and after harmonics

conditions of failure stated above, it could be observed that 61.67 % of the MOA population degraded with external harmonics in the voltage stress experienced breakdown, as compared to 45% when the voltage stress contains no external harmonic. This could further be observed in terms of the hasard or failure rate functions obtained. The failure rate function of arresters degraded without external harmonics $h_1(t)$ is observed to be sharply increasing from 0 to 2.46×10^{-4} failures per hour in the time interval $t \in [100.6; 500]$, before decreasing from 2.46×10^{-4} to 2.35×10^{-4} failures per hour across the time interval $t \in [500; 4500]$. For arrester samples degraded with external harmonics, the failure rate function $h_2(t)$ is observed to be sharply increasing from 0 to 3.33×10^{-4} failures per hour across the time interval $t \in [100.6; 500]$. Across the time interval $t \in [500; 4500]$, the failure rate $h_2(t)$ indicated a lower rate increase from 3.33×10^{-4} to 4.16×10^{-4} failures per hour. The decreasing failure rate implies early failure of arrester components in the life cycle of these components under standard service condition, while the increasing failure rate suggests a wear out of these protective devices. This therefore indicates that for the time-interval $[100.6, 4500]$, the failure rate arresters degraded without external harmonics is consistently lower than that of samples subjected to harmonics. This implies that the statement: $h_2(t) < h_1(t)$, for $t = [100.6; 4500]$ is not true and the opposite statement: $h_1(t) < h_2(t)$, for $t = [100.6; 4500]$ is therefore true. The failure rate graphs $h_1(t)$ and $h_2(t)$ are shown in figure 14.

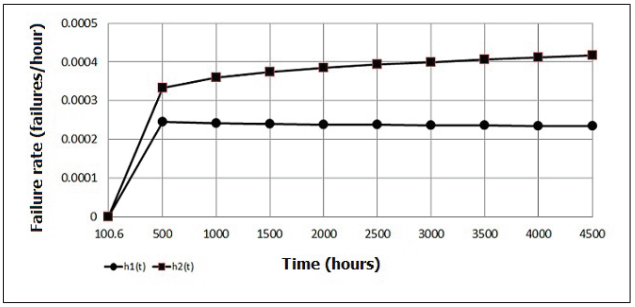

Figure 14: Failure rate function before and after harmonics

An analysis of the reliability function or the survival probability graphs obtained across $[100.6; 4500]$ time-interval, for both observed populations shows that $R_1(t)$ decays from 100 % to 36 %, while $R_2(t)$ changes from 100 %

to 17 %. Moreover, for each point in time belonging to interval $[100.6;4500]$, it is observed that $R_1(t)$ is consistently less than $R_2(t)$. Therefore, the lower reliability or probability of survival for arresters degraded with external harmonics, as compared to those degraded with no external harmonics can be associated to the content of harmonic distortion in the voltage stress. This implies the relationship: $R_1(t) > R_2(t)$, for $t = [100.6;4500]$. The reliability functions of both populations are plotted in figure 15.

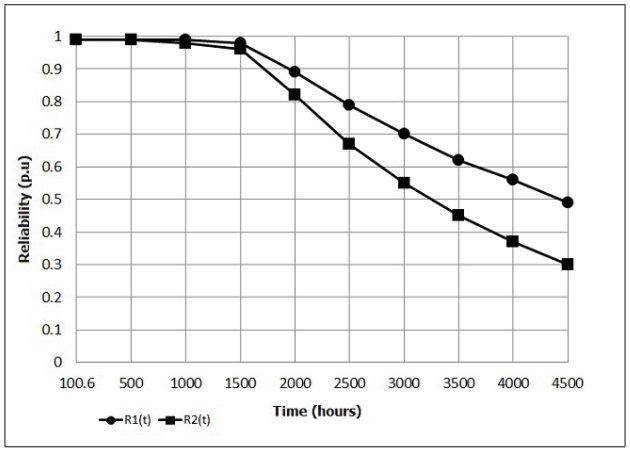

Figure 15: Reliability functions

The probability of one population of tested arresters to experience longer time to failure over the other, such as determined in equation 11, yields the probability value (Pr = 0.4107 or 41.07%), which is obviously less than 0.50 or 50%. This suggests that the time to failure or the probability of arresters, subjected to external harmonics, experiencing longer time to failure than those degraded with harmonics is 41.07%. Since the probability sum: $Pr[t_2 \geq t_1] + Pr[t_1 \geq t_2] = 1$. This therefore implies $Pr[t_1 \geq t_2]$ = 1 - $Pr[t_2 \geq t_1]$ = 0.5893 or 58.93%. This suggests that the stated relationship: $P[t_2 \geq t_1] > 0.50$ cannot be true, and consequently the probability of arresters, degraded without external harmonics, to survive longer is actually 58.93% higher.

The MTTF obtained for arresters degraded without harmonics is found to be 4252.65 hours as opposed to 2512.81 hours for those degraded with external harmonics. This demonstrates that metal oxide arresters degraded with external harmonics experienced 40.91% reduction of their lifetime, and therefore demonstrated lower reliability.

The PDF curves obtained in figure 16 show higher density of failure for the arrester components subjected to external harmonics. The magnitude of the fundamental, the 3^{rd} and 5^{th} harmonic resistive current components obtained are: 0.013 mA, 0.005 mA, 0.003 mA for arresters degraded without harmonics and 0.137 mA, 0.104 mA, 0.082 mA for those degraded with external harmonics, respectively. The resistive current component before harmonic injection is therefore 0.0143 mA and 0.191 mA after injection of external harmonics. An increase of 92.51% in the resistive current of the arrester samples degraded in the presence of external harmonics was therefore observed.

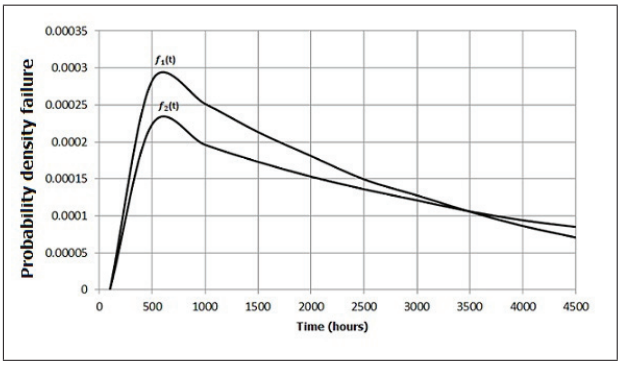

Figure 16: PDF of degraded arrester populations

It could also be noted that the fundamental and the THRC make up at least 90% of the total resistive current measured before and after harmonics injection at the same operating temperature. This shows correlation between the increase in the resistive current and the higher probability of failure, the reduced MTTF, the higher failure rate and lower reliability as well as the severe shift in the $U-I$ characteristic curve, in arrester populations subjected to external harmonics. The increase in the resistive current directly translates into increased power losses being absorbed by arrester components, which will therefore quicken the thermal runway process. Since the test temperature which represents the device's operating environment was kept constant, the rise in the resistive current and the subsequent high power losses experienced, when external harmonics are injected, could therefore be attributed to the influence of harmonic voltage frequencies on the overall continuous biasing effect of the applied voltage stress. Furthermore, the study on the degradation mechanism of metal oxide-based arresters described in [4], revealed that the degradation of these arresters consists of the resultant effect of the breakdown of several millions of individual grain boundaries at the following voltage levels: 3.02 V and 3.11 V per grain boundary, for monotonous and non-monotonous ageing process respectively. This therefore suggests that the reduced time to failure and the increased resistive current, observed in MOA samples subjected to external harmonics injection, results from the contributing effect of voltage harmonic components on the breakdown voltage between individual grain boundaries. This demonstrates that voltage harmonics could be regarded as aggravating factors of the long-term degradation phenomenon of these overvoltage protective devices. The third harmonic voltage will, by virtue of its magnitude, be the second voltage contributor to the MOA microstructure disintegration, hence to the accelerated degradation.

7. CONCLUSION

For the purpose of this work, similar arrester units are subjected to accelerated degradation test, at elevated temperature and voltage. The voltage applied is embedded with harmonics. The observed time to failure or life expectancy represents the behaviour pattern of these

overvoltage units, when operating at normal service condition with distorted voltage for a long period of time. The resistive current components as well as the $U - I$ characteristic curve confirm the the degradation status of arrester units. The following findings are obtained:

1. Continuous exposure of metal oxide-arresters to distorted ac voltage is prone to aggravate the degradation or failure process of these surge protection units.

2. The reduced time to failure or lifetime of MOA units, continuously operated under distorted ac voltage, could be attributed to additional watt loss experienced in these devices which result from increased harmonic resistive current conduction.

3. Harmonic components embedded in the voltage stress contribute to the biasing effect of MOA units.

These findings imply that the presence of harmonic components in the voltage across arrester units will fast track the disintegration process of the intergranular boundaries of MOA arresters. This therefore explains the higher probability of electrical failure or reduced life expectancy of metal oxide-based arresters under harmonic distortion conditions. The develpment of new oxide additives, capable to decelerate intergranular disintegration under the effect of voltage stress, could be recommended as one of the directions for future designs of MOAs.

REFERENCES

[1] A. Vasic, M. Vujisic and P. Osmokrovic: "Aging of overvoltage protection elements caused by past activations", *Microelectronics, Electronic Components and Materials*, Vol. 42 No. 3, pp. 197-204, October 2012.

[2] K. Eda, A. Iga and M. Matsuoka: "Degradation mechanism of non-ohmic zinc oxide ceramics", *Journal of Applied Physics*, Vol. 51 No. 5, pp. 2678-2684, January 1980.

[3] D. Zhou, C. Zhang and S. Gong: "Degradation phenomena due to dc bias in low-voltage ZnO varistors", *Materials Science and Engineering:B*, Vol. 99 No. 1-3, pp. 412-415, May 2003.

[4] J. He, J. Liu, J. Hu, R. Zeng and W. Long: "Non-uniform behaviour of individual grain boundaries in ZnO varistor ceramics", *Journal of the European Ceramic Society*, Vol. 31 No. 8, pp. 1451-1456, July 2011.

[5] C. Nahm : "Microstructure, electrical properties, and aging behaviour of ZnO-$Pr6O_{11}$-CoO-Cr_2O_3-Dy_2O_3 varistor ceramics", *Ceramics International*, Vol. 37 No. 8, pp. 3049-3054, December 2011.

[6] Z. Nanfa, K. Guoyao and G. Yaping: "Long duration impulse withstand capability of SPD", *Proceedings: the Asia-Pacific International Symposium on Electromagnetic Compatibility*, Beijing, April 2010.

[7] J. Rossman, J. Nelson and M. Droke: "Reliability and failure of porcelain high-voltage surge arresters", *Proceedings: International Conference on High Voltage Engineering and Application*, New Orleans, October 2010.

[8] V. Hinrichsen: "Monitoring of high voltage metal oxide surge arresters", *Proceedings: 6th International Conference on Electrical Insulation*, Bilbao, October 1997.

[9] M. Jaroszewsky, P. Kostyla and K. Wieczorek: "Effect of voltage harmonics content on arrester diagnostic result", *Proceedings: International Conference on Solid Dielectrics*, Toulouse, July 2004.

[10] V. Larsen and K. Lien: "In-service testing and diagnosis of gapless metal oxide surge arresters", *Proceedings: 9th International Symposium on Lightning Protection*, Foz do Iguacu, November 2007.

[11] P. Bokoro, M. Hove and I. Jandrell: "Statistical analysis of MOV leakage current under distorted supply voltage conditions", *Proceedings: IEEE Electrical Insulation Conference*, Philadelphia, June 2014.

[12] R. Hernandez, I. Ramrez, R. Saldivar and G. Montoya: "Analysis of accelerated ageing of non-ceramic insulation equipments", *Generation, Transmission and Distribution, IET*, Vol. 6 No. 1, pp. 59-68, January 2012.

[13] Nabertherm GmbH: *High temperature laboratory furnace operating manual*, http://www.nabertherm.com. 2011.

[14] IEEE P519.1/D12: *Guide for Applying Harmonic Limits on Power Systems*, IEEE Power Standards Coordinating Committee, November 2012.

[15] Lapp Cables Group: *High temperature cables operating instructions*, http://www.lappkabel.co.za. 2013.

[16] IEEE 930^{TM}: *IEEE guide for the statistical analysis of electrical insulation breakdown data*, IEEE Standards 2007.

[17] Epcos data book: *SIOV Metal Oxide Varistors*, pp. 51-52, http://www.epcos.com. 2008.

[18] M.Wang, Q.Tang, and C.Yao: "Electrical properties and ac degradation characteristics of low voltage ZnO varistors doped with Nd_2O_3", *Ceramics International*, Vol. 36 No. 3, pp. 1095-1099, January 2010.

[19] J. He, J. Liu, J. Hu, and W. Long: "AC ageing characteristics of Y_2O_3-doped ZnO varistors with high voltage gradient", *Materials Letters*, Vol. 65 No. 17-18, pp. 2595-2597, September 2011.

[20] IEEE C62.11: *IEEE standard for metal oxide surge arresters for ac power circuits higher than 1 kV*, IEEE Standards 1999.

[21] J. White : "The moments of log-Weibull order statistics", *Techtometrics*, Vol. 11 No. 2, pp. 373-386, February 1969.

[22] H. Yahyaoui, P. Notingher, S. Angel and Y. Kieffel: "Proprietes dielectriques d'une resine epoxy d'alumine sous l'effet du champ electrique continu et de la temperature", *Proceedings: Journees JCGE' 2014-SEEDS*, http://www.hal.archives-ouvertes.fr/hal-01083915, June 2014.

[23] P. D. O'connor and A. Kleyner: *Practical Reliability*, John Wiley and Sons, UK, fifth edition, chapter 3, pp. 87-92, August 2011.

[24] A. S. Yahaya, C. S. Yee, N. A. Ramli and F. Ahmad: "Determination of the best probability plotting position for predicting parameters of the weibull distribution", *International Journal of Applied Science and Technology*, Vol. 2 No. 3, pp. 106-112, March 2012.

[25] G. G. Brown and H. C. Rutemiller: "Evaluation of $\Pr\{X \geq Y\}$ when both X and Y are three-parameter weibull distributions", *IEEE Transactions on Reliability*, Vol. R.22 No. 2, pp. 78-82, June 1973.

[26] M. Kayid, I. A. Ahmad, S. Izadkhah and A. M. Abouammoh: "Further results involving the mean time to failure order, and the decreasing mean time to failure class", *IEEE Transactions on Reliability*, Vol. 62 No. 3, pp. 670-678, September 2013.

[27] C. Karawita and M. Raghuveer: "Leakage current based assessment of degradation of MOSA using an alternative technique", *Proceedings: Annual Report of the Conference on Electrical Insulation and Dielectric Phenomena (CEIDP)*, October 2005.

[28] Z. Abdul-Malek, N. Yusof and M. Yousof: "Field experience on surge arrester condition monitoring modified shifted current method", *Proceedings: 45th Universities Power Engineering Conference (UPEC)*, Cardiff, 2010.

[29] X. Yan, Y. Wen and X. Yi: "Study on the resistive leakage current characteristic of MOV surge Arresters", *Proceedings: Asia-Pacific IEEE/PES Transmission and Distribution Conference and Exhibition*, Yokohama, October 2002.

[30] M. Khodsuz, M. Mirzaie and S. Seyyedbarzegar: "Metal oxide surge arrester condition monitoring based on analysis of leakage current components", *International Journal of Electrical Power and Energy Systems*, Vol. 12 No. 6, pp. 188-193, November 2014.

[31] E. Shulzhenko, M. Rock, M. Birle and C. Leu: "Applying of surge arresters in power electronic network components", *Proceedings: the International Conference on Lightning Protection*, Shanghai, October 2014.